

# Crack detection in rectangular plate by electromechanical impedance method: modeling and experiment

Mehdi Rajabi<sup>1,2</sup>, Mahnaz Shamsirsaz<sup>\*2</sup> and Mahyar Naraghi<sup>1</sup>

<sup>1</sup>Department of Mechanical Engineering, Amirkabir University of Technology, Tehran, Iran

<sup>2</sup>New Technologies Research Center, Amirkabir University of Technology, Tehran, Iran

(Received August 23, 2016, Revised January 22, 2017, Accepted February 2, 2017)

**Abstract.** Electromechanical impedance method as an efficient tool in Structural Health Monitoring (SHM) utilizes the electromechanical impedance of piezoelectric materials which is directly related to the mechanical impedance of the host structure and will be affected by damages. In this paper, electromechanical impedance of piezoelectric patches attached to simply support rectangular plate is determined theoretically and experimentally in order to detect damage. A pairs of piezoelectric wafer active sensor (PWAS) patches are used on top and bottom of an aluminum plate to generate pure bending. The analytical model and experiments are carried out both for undamaged and damaged plates. To validate theoretical models, the electromechanical impedances of PWAS for undamaged and damaged plate using theoretical models are compared with those obtained experimentally. Both theoretical and experimental results demonstrate that by crack generation and intensifying this crack, natural frequency of structure decreases. Finally, in order to evaluate damage severity, damage metrics such as Root Mean Square Deviation (RMSD), Mean Absolute Percentage Deviation (MAPD), and Correlation Coefficient Deviation (CCD) are used based on experimental results. The results show that generation of crack and crack depth increasing can be detectable by CCD.

**Keywords:** electromechanical impedance method; Structural Health Monitoring; damage index; crack intensity; thin plate; modeling; experiments

## 1. Introduction

Impedance based structural health monitoring (SHM) using piezoelectric wafer active sensor (PWAS) as a sensor and actuator is a powerful technique in damage detection (Lee *et al.* 2016, Min *et al.* 2016, Min *et al.* 2015, Lim and Soh 2013). This method is based on the measurement of the electromechanical impedance of piezoelectric patch attached to the structure. Liang *et al.* (1994), showed that the electromechanical admittance  $Y$  which is an inverse of the electromechanical impedance of the PWAS actuator is a combined function of the mechanical impedance of the PWAS actuator and that of the host structure. Any change in the host structure will change the electromechanical impedance of the PWAS. In a study carried out by Wang *et al.* (1996), the dependence of the electromechanical admittance on the structural impedance is once again observed, which confirms a possibility of monitoring structural behavior by measuring the electromechanical admittance of the PWAS. Wang *et al.* (1997), investigated the deformation compatibility of piezoelectric patches with a beam or plate. In SHM using electromechanical impedance method, however several theoretical models have been developed for undamaged structures (Giurgiutiu and Zagrai 2002, Zagrai and Giurgiutiu 2001, Li *et al.* 2005,

Sepehry *et al.* 2011, Sepehry *et al.* 2014, Rugina *et al.* 2015) but few studies are focused on damaged structures (Tseng and Wang 2005, Yan *et al.* 2007).

Giurgiutiu and Zagrai (2002) presented a theoretical model related to coupling effect between piezoelectric patch and beam in which the effect of piezoelectric patch has been considered by exerting moment and force on beam. At first, they derived the impedance for a constrained piezoelectric in which constraints were applied by structure stiffness. Then structure stiffness was calculated and substituted in impedance equation. Zagrai and Giurgiutiu (2001) analyzed a 2-D circular plate analytically and experimentally where both axial and flexural components of natural vibrations were included. Li *et al.* (2005) presented the electromechanical impedance of thin rectangular plate with piezoelectric actuator and used a pair of piezoelectric patch to produce pure bending. Sepehry *et al.* (2014) modeled effect of temperature on electromechanical impedance of rectangular plate. Rugina *et al.* (2015) studied effect of damage on electromechanical impedance of circular plate using FEM. Tseng and Wang (2005) presented a two-dimensional electromechanical impedance model to predict admittance of the PWAS transducer bonded to the plate. They presented a model considering square damage on plate. Yan *et al.* (2007) presented a theoretical model for undamaged and damaged beam. Damage was modeled by exerting change in Young's modulus in the damaged area.

In this paper, an electromechanical impedance model is derived for simply supported rectangular thin plate with a pair of the PWAS patch bonded at top and bottom of the

\*Corresponding author, Professor  
E-mail: [shams Shir@aut.ac.ir](mailto:shams Shir@aut.ac.ir)

plate in order to detect crack damage. The analytical model is based on flexural vibration of the plate. The crack with an arbitrary length, depth located in parallel to one side of the aluminum plate is generated artificially. The analytical model and experiments were carried out first for plate without damage and second for damaged plates with crack. The electromechanical impedances of PWAS for undamaged and damaged plate obtained by theoretical model are compared with those obtained experimentally. In order to examine effect of crack intensity on electromechanical impedance of structure, three different damage metrics: Root Mean Square Deviation (RMSD), the Mean Absolute Percentage Deviation (MAPD), and Correlation Coefficient Deviation (CCD) are used to evaluate damage severity quantitatively.

## 2. Electromechanical impedance model

Consider a plate with PWAS patches bonded on both sides of it (Fig. 1). The PWAS patches have length of  $a_p$ , width of  $b_p$  and with  $h_p$  thickness. The sides of attached PWAS are parallel to sides of the plate (Fig. 1). Similar to the model presented in (Tseng and Wang 2005), the interaction between PWAS and plate is modeled by considering an effective structural dynamic stiffness in  $x$  and  $y$  direction exerted on PWAS by plate (Fig. 2).

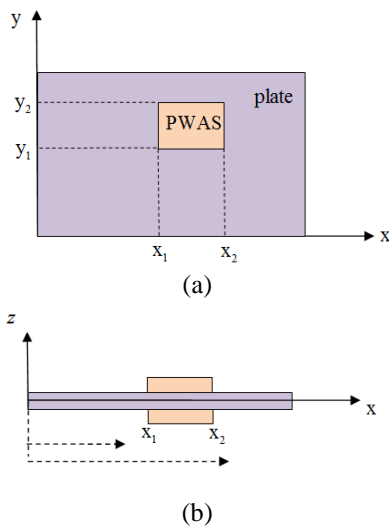


Fig. 1 Plate with attached PWAS a) in  $x$ - $y$  plane, b) in  $x$ - $z$  plane

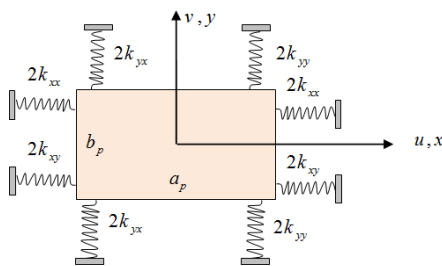


Fig. 2 The interaction of two-dimensional PWAS on plate

The constitutive equations of the PWAS patch are

$$\begin{aligned} S_x &= \frac{1}{\bar{E}_p}(T_x - \nu_p T_y) + d_{31}E, \\ S_y &= \frac{1}{\bar{E}_p}(T_y - \nu_p T_x) + d_{32}E, \\ D_z &= \bar{\epsilon}_{33}^T E + d_{31}T_x + d_{32}T_y, \end{aligned} \quad (1)$$

Where  $S_x$  and  $S_y$  are the strains,  $T_x$  and  $T_y$  are the stress,  $d_{31}$  and  $d_{32}$  are the piezoelectric constants in  $x$  and  $y$  directions respectively.  $\bar{\epsilon}_{33}^T = \epsilon_{33}^T(1 - \delta j)$  is the dielectric constant at zero stress,  $\delta$  represents the dielectric loss factor, and  $\bar{E}_p = E_p(1 + \eta j)$  is the elastic modulus at zero electric field,  $\eta$  is the mechanical loss factor and  $D$  is the electric displacement.

Equations of motion of the PWAS patch can be described by the following equations

$$\begin{aligned} \frac{\bar{E}_p}{1 - \nu_p^2} \frac{\partial^2 u}{\partial x^2} &= \rho_p \frac{\partial^2 u}{\partial t^2}, \\ \frac{\bar{E}_p}{1 - \nu_p^2} \frac{\partial^2 v}{\partial y^2} &= \rho_p \frac{\partial^2 v}{\partial t^2}. \end{aligned} \quad (2)$$

Where  $u$  and  $v$  are displacement responses in  $x$  and  $y$  directions respectively, and  $\rho_p$  is the density of the PWAS patch. One can obtain solution of Eq. (2) as

$$\begin{aligned} u(x, y) &= (c_1 \sin kx + c_2 \cos ky) e^{j\omega t}, \\ v(x, y) &= (c_3 \sin kx + c_4 \cos ky) e^{j\omega t}, \end{aligned} \quad (3)$$

Where  $k$  is a wave number,  $\omega$  is the excitation frequency,  $t$  is time,  $c_1$ ,  $c_2$ ,  $c_3$  and  $c_4$  are constants to be determined applying boundary conditions. Because of symmetrical displacement, boundary conditions at the center of PWAS are

$$u|_{x=0} = 0 \text{ and } v|_{y=0} = 0 \quad (4)$$

At the boundaries  $x = a_p/2$  and  $y = b_p/2$ , we have

$$\begin{bmatrix} F_x \\ F_y \end{bmatrix} = \begin{bmatrix} T_x b_p h_p \\ T_y a_p h_p \end{bmatrix} = - \begin{bmatrix} 2k_{xx} & 2k_{xy} \\ 2k_{yx} & 2k_{yy} \end{bmatrix} \begin{bmatrix} u \\ v \end{bmatrix}. \quad (5)$$

By applying boundary conditions to Eq. (3), unknown constants can be determined as

$$\begin{aligned} c_1 &= (N_{11} d_{31} + N_{12} d_{32}) E / k, & c_2 &= 0, \\ c_3 &= (N_{21} d_{31} + N_{22} d_{32}) E / k, & c_4 &= 0, \end{aligned} \quad (6)$$

Where

$$N = \begin{bmatrix} N_{11} & N_{12} \\ N_{21} & N_{22} \end{bmatrix} = \begin{bmatrix} \cos \varphi_1 (1 - \nu_p \frac{b_p k_{yx}}{a_p k_{px}} + \frac{k_{xx}}{k_{px}}) & \cos \varphi_2 (\frac{a_p k_{xy}}{b_p k_{py}} - \nu_p \frac{k_{yy}}{k_{py}}) \\ \cos \varphi_1 (\frac{b_p k_{yx}}{a_p k_{px}} - \nu_p \frac{k_{xx}}{k_{px}}) & \cos \varphi_2 (1 - \nu_p \frac{a_p k_{xy}}{b_p k_{py}} + \frac{k_{yy}}{k_{py}}) \end{bmatrix} \quad (7)$$

Where  $\varphi_1 = ka_p/2$ ,  $\varphi_2 = kb_p/2$ ,  $k_{px} = \bar{E}_p h_p \varphi_1 / \tan(\varphi_1)$ , and  $k_{py} = \bar{E}_p h_p \varphi_2 / \tan(\varphi_2)$ . By substitution of Eq. (3) in Eq. (1), the electric current passing through the PWAS patch can be obtained

$$I = j\omega \int_{A_p} D dx dy = j\omega E a_p b_p \left\{ \frac{d_{31}^2 \bar{E}_p}{1-\nu_p} (2 - (N_{11} + N_{21}) \frac{\sin \varphi_1}{\varphi_1} - (N_{21} + N_{22}) \frac{\sin \varphi_2}{\varphi_2}) \right\}. \quad (8)$$

The electric field in the thickness direction of the PWAS is  $E = V e^{j\alpha x} / h_p$ , where  $V$  is voltage applying on PWAS. Electromechanical impedance of the PWAS patch can be determined as

$$Z = \frac{V}{I} = \frac{1}{j\omega C} \left\{ 1 - \frac{d_{31}^2 \bar{E}_p}{(1-\nu_p) \bar{E}_{33}} (2 - (N_{11} + N_{21}) \frac{\sin \varphi_1}{\varphi_1} - (N_{21} + N_{22}) \frac{\sin \varphi_2}{\varphi_2}) \right\}^{-1}. \quad (9)$$

where  $\varphi_2 = kb_p / 2$  is the conventional capacitance of the PWAS patch.

### 2.1 Structural stiffness of undamaged plate

Considering simply supported rectangular plate vibration by a pair of PWAS patches, the theory of thin plates can be adopted (Fig. 3). The equation of motion for force vibration of thin plate can be expressed as follow

$$D \left( \frac{\partial^4 w}{\partial x^4} + 2 \frac{\partial^4 w}{\partial x^2 \partial y^2} + \frac{\partial^4 w}{\partial y^4} \right) + \rho H \ddot{w} = \frac{\partial^2 \bar{M}_x}{\partial x^2} + \frac{\partial^2 \bar{M}_y}{\partial y^2}, \quad (10)$$

where  $D = E_{plate} H^3 / 12(1-\nu^2)$ ,  $E_{plate}$  Young's modulus,  $H$  is thickness,  $\nu$  is poisson's ratio and  $\bar{M}_x$  and  $\bar{M}_y$  are moments inserted by PWAS on plate and are described by

$$\begin{aligned} \bar{M}_x &= \bar{M}_{px} [L(x-x_1) - L(x-x_2)] [L(y-y_1) - L(y-y_2)] \\ \bar{M}_y &= \bar{M}_{py} [L(x-x_1) - L(x-x_2)] [L(y-y_1) - L(y-y_2)] \end{aligned} \quad (11)$$

where  $\bar{M}_{px} = 2F_{px} e^{j\alpha x} \times \frac{H}{2}$  and  $\bar{M}_{py} = 2F_{py} e^{j\alpha x} \times \frac{H}{2}$ , and  $L(\cdot)$  is Heaviside step function.

The solution of Eq. (10) is assumed as follow

$$w(x, y, t) = \sum_{m,n=0}^{\infty} \phi_{mn} W_{mn}(x, y) e^{j\alpha t}, \quad (12)$$

Where  $W_{mn}(x, y) = \frac{2}{\sqrt{\rho H a b}} \sin \frac{m\pi}{a} x \sin \frac{n\pi}{b} y$  are mode shape functions of rectangular simply supported plate in which  $a$  and  $b$  are length and width of the plate respectively.

By substitute Eq. (11) and Eq. (12) in Eq. (10),  $\phi_{mn}$  can be obtained as follow

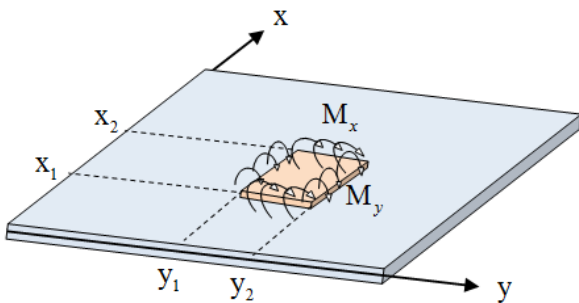


Fig. 3 Effect of PWAS pairs by exerted moment on plate

$$\phi_{mn} = \frac{2I_x I_y}{\rho m n \pi^2 (\omega_{mn}^2 - \omega^2 + 2\zeta_f \omega_{mn} \omega j)} \left[ \left( \frac{m\pi}{a} \right)^2 F_{px} + \left( \frac{n\pi}{b} \right)^2 F_{py} \right], \quad (13)$$

where  $I_x = \cos \frac{m\pi}{a} x_1 - \cos \frac{m\pi}{a} x_2$ ,  $I_y = \cos \frac{n\pi}{b} y_1 - \cos \frac{n\pi}{b} y_2$ ,  $\zeta_f$  are damping coefficients, and  $\omega_{mn} = \pi^2 \left( \left( \frac{m}{a} \right)^2 + \left( \frac{n}{b} \right)^2 \right) \sqrt{\frac{D}{\rho H}}$  are natural frequencies of rectangular plate.

The relation between the total displacement of the PWAS and plate deflection can be expressed as

$$\begin{aligned} u_p &= -\frac{H}{2} \left( \frac{\partial w}{\partial x} \Big|_{x=x_2} - \frac{\partial w}{\partial x} \Big|_{x=x_1} \right) \Big|_{y_1}^2, \\ v_p &= -\frac{H}{2} \left( \frac{\partial w}{\partial y} \Big|_{y=y_2} - \frac{\partial w}{\partial y} \Big|_{y=y_1} \right) \Big|_{x_1}^2. \end{aligned} \quad (14)$$

Where  $u_p$  and  $v_p$  are the total displacements of the PWAS in  $x$  and  $y$  directions respectively. By substitute Eq. (11) in Eq. (14), one can obtain the relation between displacements and forces as follow

$$\begin{Bmatrix} F_{px} \\ F_{py} \end{Bmatrix} = \frac{2}{H} \begin{bmatrix} H_{xx} & H_{xy} \\ H_{yx} & H_{yy} \end{bmatrix}^{-1} \begin{Bmatrix} u_p \\ v_p \end{Bmatrix} \quad (15)$$

where

$$\begin{aligned} H_{xx} &= \frac{2b}{\rho a^3 b_p} \sum_{m,n=0}^{\infty} \frac{m^2}{n} \frac{I_x^2 I_y^2}{\omega_{mn}^2 - \omega^2 + 2\zeta_f \omega_{mn} \omega j} \\ H_{xy} &= \frac{2}{\rho a b b_p} \sum_{m,n=0}^{\infty} n \frac{I_x^2 I_y^2}{\omega_{mn}^2 - \omega^2 + 2\zeta_f \omega_{mn} \omega j} \\ H_{yx} &= \frac{2}{\rho a b a_p} \sum_{m,n=0}^{\infty} m \frac{I_y^2 I_x^2}{\omega_{mn}^2 - \omega^2 + 2\zeta_f \omega_{mn} \omega j} \\ H_{yy} &= \frac{2a}{\rho b^3 a_p} \sum_{m,n=0}^{\infty} \frac{n^2}{m} \frac{I_y^2 I_x^2}{\omega_{mn}^2 - \omega^2 + 2\zeta_f \omega_{mn} \omega j} \end{aligned} \quad (16)$$

From Eq. (14), the dynamic stiffness of the plate is obtained as follow

$$\begin{bmatrix} k_{xx} & k_{xy} \\ k_{yx} & k_{yy} \end{bmatrix} = \frac{1}{H} \begin{bmatrix} H_{xx} & H_{xy} \\ H_{yx} & H_{yy} \end{bmatrix}^{-1} \quad (17)$$

### 2.2 Structural stiffness of damaged plate

Consider a simply supported rectangular plate driven by a pair of PWAS and a crack as shown in Fig. 4. The coordinates of the crack center are  $x_0$  and  $y_0$ , crack length is  $C$  and  $\xi = h/H$  is crack relative depth at its center. For calculate natural frequency and mode shape functions, plate is divided in two regions from crack line and vibration of two plates is considered. Then vibrations of two separate plates are studied by applying consistency of boundary conditions. The equation for the free vibration of plate is given by (Khadem and Rezaee 2000)

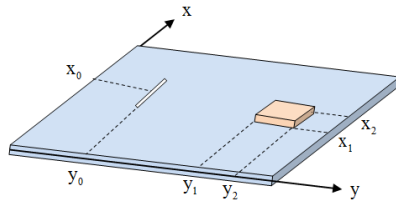


Fig. 4 Rectangular plate with finite length crack and PWAS patch

$$D \left( \frac{\partial^4 w}{\partial x^4} + 2 \frac{\partial^4 w}{\partial x^2 \partial y^2} + \frac{\partial^4 w}{\partial y^4} \right) + \rho H \ddot{w} = 0. \quad (18)$$

Consider  $w(x, y, t) = W(x, y)e^{i\omega t}$  and substitute in Eq. (18), one may obtain

$$\frac{\partial^4 W}{\partial \eta^4} + 2\phi^2 \frac{\partial^4 W}{\partial \eta^2 \partial \zeta^2} + \phi^4 \frac{\partial^4 W}{\partial \zeta^4} - \lambda^4 \phi^4 W = 0, \quad (19)$$

Where  $\zeta = x/a$  and  $\eta = y/b$  are dimensionless coordinates in  $x$  and  $y$  directions, respectively,  $\lambda^4 = \rho H \omega^2 / D$ , and  $\phi = b/a$ . The solution of Eq. (19) may be expressed as

$$W(\zeta, \eta) = \sum_{m=1}^{\infty} Y_m(\eta) \sin(m\pi\zeta) \quad (20)$$

Substitute in Eq. (20) in Eq. (19), the solution of  $Y_m(\eta)$  for two regions of plate may be expressed as

$$\begin{aligned} Y_{1m}(\eta) &= A_1 \cosh(\beta_m \eta) + A_2 \sinh(\beta_m \eta) + A_3 \cos(\gamma_m \eta) + A_4 \sin(\gamma_m \eta) \quad 0 < \eta < \eta_0 \\ Y_{2m}(\eta) &= B_1 \cosh(\beta_m \eta) + B_2 \sinh(\beta_m \eta) + B_3 \cos(\gamma_m \eta) + B_4 \sin(\gamma_m \eta) \quad \eta_0 < \eta < 1 \end{aligned} \quad (21)$$

where  $\beta_m = \phi \sqrt{\lambda^2 + (m\pi)^2}$ ,  $\gamma_m = \phi \sqrt{\lambda^2 - (m\pi)^2}$ , and  $A_1$ - $A_4$ ,  $B_1$ - $B_4$  are constants. Non-dimensional compliance coefficient at the crack center is

$$\alpha_{bb}^0 = \frac{1}{H} \int_0^h \xi (1.99 - 2.47\xi + 12.97\xi^2 - 23.11\xi^3 + 24.8\xi^4)^2 dh \quad \xi = h/H \quad (22)$$

where  $h$  is the depth of crack. The existent of the crack cause the slope discontinuity at both side of crack, and is calculated as (Khadem and Rezaee 2000)

$$\theta|_{\eta=\eta_0} = \frac{-6H}{ab} \left( \frac{\partial^2 w}{\partial \eta^2} + \nu \phi^2 \frac{\partial^2 w}{\partial \zeta^2} \right) \alpha_{bb}^0 E(\zeta) f(\zeta) |_{\eta=\eta_0}, \quad (23)$$

where

$$E(\zeta) = \frac{2C/H + 3(3+\nu)(1-\nu)\alpha_{bb}^0(1-f(\zeta))}{2C/H + 3(3+\nu)(1-\nu)} f(\zeta) = e^{-\nu^2(\zeta-\zeta_0)^2/2(c/a)^2} \quad (24)$$

Boundary conditions at the crack location  $\eta = \eta_0$ , may be expressed as follow

$$\begin{aligned} W_1 &= W_2 \rightarrow Y_1 = Y_2 \\ M_1 &= M_2 \rightarrow \frac{d^2 Y_1}{d\eta^2} - \phi^2 \nu (m\pi)^2 Y_1 = \frac{d^2 Y_2}{d\eta^2} - \phi^2 \nu (m\pi)^2 Y_2 \\ V_1 &= V_2 \rightarrow \frac{dY_1}{d\eta} - \phi^2 (2-\nu)(m\pi)^2 \frac{dY_1}{d\eta} = \frac{dY_2}{d\eta} - \phi^2 (2-\nu)(m\pi)^2 \frac{dY_2}{d\eta} \\ \frac{dW_1}{d\eta} - \theta &= \frac{dW_2}{d\eta} \rightarrow \frac{dY_1}{d\eta} + \frac{6H}{ab} \left( \frac{dY_1}{d\eta} - \phi^2 \nu (m\pi)^2 Y_1 \right) \alpha_{bb}^0 E(\zeta) f(\zeta) = \frac{dY_2}{d\eta} \end{aligned} \quad (25)$$

By applying boundary conditions one may obtain eigenvalue problem. Mode shape functions may be expressed with solving the eigen functions as

$$\begin{aligned} W_{1m}(\zeta, \eta) &= A_{2m} \left( \sinh \beta_m \eta + \frac{e_3 + e_4 E(\zeta) f(\zeta)}{e_5 E(\zeta) f(\zeta)} \sin \gamma_m \eta \right) \sin \frac{m\pi}{a} \zeta \\ W_{2m}(\zeta, \eta) &= (e_1 \sinh \beta_m (\eta - 1) + e_2 \frac{e_3 + e_4 E(\zeta) f(\zeta)}{e_5 E(\zeta) f(\zeta)} \sin \gamma_m (\eta - 1)) \sin \frac{m\pi}{a} \zeta \end{aligned} \quad (26)$$

where in which

$$\begin{aligned} e_1 &= \frac{\sinh \beta_m \eta_0}{\sinh \beta_m (\eta_0 - 1)}, e_2 = \frac{\sin \gamma_m \eta_0}{\sin \gamma_m (\eta_0 - 1)}, \\ e_3 &= 2\beta_m \phi^2 \lambda^2 \left[ \cosh \beta_m \eta_0 - \frac{\sinh \beta_m \eta_0 \cosh \beta_m (\eta_0 - 1)}{\sinh \beta_m (\eta_0 - 1)} \right], \\ e_4 &= \frac{6H}{b} \alpha_{bb}^0 \lambda_1^2 \sinh \beta_m \eta_0, e_5 = \frac{6H}{b} \alpha_{bb}^0 \lambda_1 \lambda_2 \sin \gamma_m \eta_0, \end{aligned} \quad (27)$$

Eigenvalues  $\lambda$ , are a function of coordinate  $\zeta$ , and begin its maximum value  $\lambda_l$  at two end of the crack and reaches in minimum value  $\lambda_d$  at the center of crack.  $\lambda_l$  and  $\lambda_d$  are eigenvalues at  $\zeta = \zeta_0$  and  $\zeta$  belong to vary at the cracked center, respectively. Calculation of  $\lambda$  is time-consuming. For this reason, Khadem and Rezaee (2000) used a modified comparison functions for approximate eigenvalues as follow

$$\lambda(\zeta) = \lambda_l - (\lambda_l - \lambda_d) e^{-(\eta-\eta_0)^2/c^2} e^{-(\zeta-\zeta_0)^2 CF/c^2}, \quad (28)$$

where  $c = C/a$ . One can use energy method to calculate natural frequencies. The maximum reference kinetic and potential energy of a rectangular plate in dimensionless coordinate can be obtained as

$$\begin{aligned} PE &= \frac{D}{2\phi_A} \left[ \phi^2 \left( \frac{\partial^2 W}{\partial \zeta^2} \right)^2 + \frac{1}{\phi} \left( \frac{\partial^2 W}{\partial \eta^2} \right)^2 + 2\nu \phi \frac{\partial^2 W}{\partial \eta^2} \frac{\partial^2 W}{\partial \zeta^2} + 2(1-\nu^2) \left( \frac{\partial^2 W}{\partial \zeta \partial \eta} \right)^2 \right] dA \\ KE^* &= \frac{1}{2} M \phi \alpha^4 \int W^2 dA \end{aligned} \quad (29)$$

The stored potential energy at the crack location may be expressed as

$$P_c = \frac{6HD \alpha_{bb}^0}{b^2 \phi^2} \int_0^1 \left( \frac{\partial^2 W_1}{\partial \eta^2} + \nu \phi^2 \frac{\partial^2 W_1}{\partial \zeta^2} \right)^2 E(\zeta) f(\zeta) d\zeta |_{\eta=\eta_0} \quad (30)$$

Therefore, natural frequency may be calculated as follow

$$\omega = \sqrt{\frac{PE_1 + PE_2 + P_c}{KE_1^* + KE_2^*}}. \quad (31)$$

Where  $PE_1$  and  $PE_2$  are maximum potential energy for region 1 and 2, respectively, and  $KE_1$  and  $KE_2$  are reference kinetic energy for region 1 and 2, respectively.

Assume that, the PWAS bonded on the plate at region two. By calculation of natural frequencies and mode shapes for two regions of the plate, and substituting in Eq. (11),  $\phi_{mn}$  may be expressed for the cracked plate as follow

$$\begin{aligned} \phi_{mn2} &= \frac{1}{\omega_{cnn}^2 - \omega^2 + 2\omega_{cnn} \omega \zeta_f j} (Q_1 \bar{M}_{px} + Q_2 \bar{M}_{py}), \\ \phi_{mn1} &= 0, \end{aligned} \quad (32)$$

Where  $\omega_{cmn}$  is natural frequency for cracked plate, and  $Q_1$  and  $Q_2$  are listed in appendix. Substituting  $w$  in Eq. (13), one can obtain the dynamic stiffness of the cracked plate as

$$\begin{bmatrix} k_{xx} & k_{xy} \\ k_{yx} & k_{yy} \end{bmatrix} = \frac{1}{H} \begin{bmatrix} \sum_{m,n=0}^{\infty} Q_1 A_1 & \sum_{m,n=0}^{\infty} Q_2 A_1 \\ \sum_{m,n=0}^{\infty} Q_1 A_2 & \sum_{m,n=0}^{\infty} Q_2 A_2 \end{bmatrix}^{-1} \quad (33)$$

Where  $A_1$  and  $A_2$  are listed in appendix A.

PWAS impedance of plate structure can be calculated by proceeding following steps:

1. Calculation of dynamic stiffness of plate using Eq. (13) for undamaged plate and Eq. (33) for damaged plate
2. Calculation of matrix N using Eq. (7) for undamaged and damaged plate.
3. Calculation of electromechanical impedance of PWAS using Eq. (9) for undamaged and damaged plate.

### 3. Results and discussion

The experimental tests are carried out on simply support rectangular plates (Fig. 5). Three aluminum plates named plate 1, 2 and 3 were selected as test specimens. Theoretically obtained data of impedance real parts of undamaged as well as damaged plate 1 are compared with those of obtained experimentally in order to validate theoretical model. To investigate effect of damage intensity and location on damage index, experimental tests are performed on plate 1, 2 and 3 by generating different damage intensities and locations. Each of plates has the dimensions of  $200 \times 200 \times 3$  mm<sup>3</sup>. Elasticity module and density of aluminum plate are considered  $E=68.6 \times 10^9$  Pa, and  $\rho=2707$  kg/m<sup>3</sup> respectively. A pair of PWAS patches was symmetrically bonded on the top and bottom surface of the plates (Fig. 5). The size of PWAS patch is  $10 \times 10 \times 0.278$  mm<sup>3</sup> and its center is located in  $x=100$  mm and  $y=155$  mm. Material properties of the PWAS (PSI 5H4E) are listed in Table 1. Impedance measurement of PWAS was carried out using an AD 5933 board.

#### 3.1 Validation of theoretical model with experimental measurements for undamaged plates

The frequency range of 20-30 kHz is selected to perform the experimental tests as a greater dynamic interaction between PWAS and structure is obtained with 20-30 peaks (Tarazaga *et al.* 2006). Fig. 6 shows real part of impedance for undamaged plates in this frequency range. In Fig. 6, real parts of impedances obtained by theoretical model are compared with those obtained by experimental measurements. In fact, however two PWAS are attached on the top and bottom of plate at same geometrical locations to produce only flexural modes but as the dimensions of these PWAS and their positions on plate cannot be exactly the same, unwanted in-plane natural frequencies can be generated in test specimen. This is why some frequency peaks in the experimental impedance spectrum are observed

Table 1 Material properties of the PWAS (PSI 5H4E)

Property	Symbol	Value
In plane compliance	$s_{11}^E$	$16.1 \times 10^{-12}$ Pa <sup>-1</sup>
In plane induced strain coefficient	$d_{31}$	$-320 \times 10^{-12}$ m/V
Dielectric constant	$\epsilon_{33}^T$	$33.63 \times 10^{-9}$ F/m
Density	$\rho_p$	7800 kg/m <sup>3</sup>

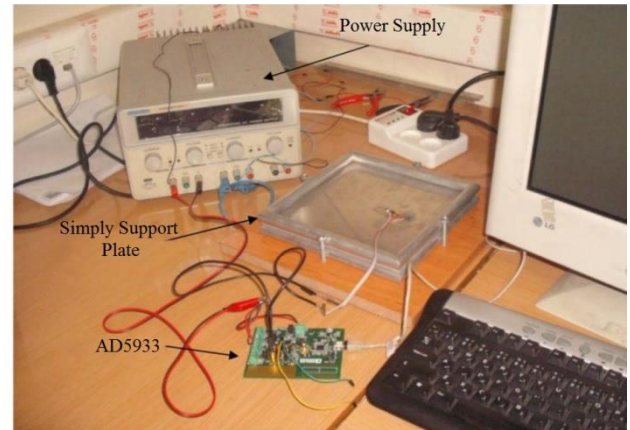


Fig. 5 Photography of plates 1, 2 and 3 with attached PWAS patches (undamaged state)

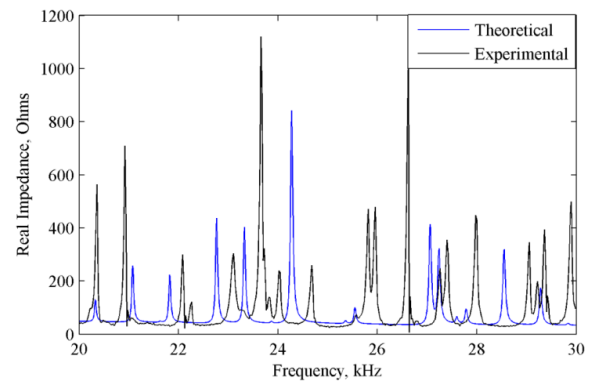


Fig. 6 Impedance spectrum obtained by theoretical model and by experiments for undamaged plate

Table 2 Natural frequencies obtained by theoretical model and by experimental tests for undamaged plate (from 20 to 30 kHz)

Experimental Freq.(kHz)	Theoretical Freq. (kHz)	Deviation %	Experimental Freq. (kHz)	Theoretical Freq. (kHz)	Deviation %
20.31	20.32	0.0492	25.86	25.55	1.2133
20.84	21.07	1.0915	26.52	-	-
21.99	-	-	27.14	27.07	0.2585
22.13	21.82	1.4207	27.3	27.24	0.2202
23.02	22.76	1.1423	27.82	27.79	0.1079
23.58	23.32	1.1149	28.93	28.54	1.3665
23.96	23.88	0.3350	29.17	-	-
24.62	24.27	1.4421	29.73	29.32	1.3847
25.7	25.36	1.3406			

(at 21.99, 26.52 and 29.17 kHz) whereas these frequency peaks are not visible in impedance spectrum by theoretical model. To compare natural frequencies obtained by theoretical model with experimental ones, their numerical values are given in Table 2. Natural frequencies measured by experiments given in Table 2 are the mean of the resonance peaks related to three plates 1, 2 and 3. There exists acceptable agreement between the theoretical and experimental resonance frequencies; the deviation of theoretical results from experimental data remains almost under 1.44%.

### 3.2 Validation of theoretical model with experimental measurements for damaged plates

Experiments were performed on same aluminum plates which are in this step subjected to artificially generated crack. First, crack is generated parallel to  $x$  axis with its center at position  $x_0=100$  mm and  $y_0=40$  mm on the plate 1. This crack has the length of 20 mm and width of 0.8 mm. Then, this crack is intensified by increasing the depth of crack in three step:  $h=1$ , 1.5 and 2 mm. For each depth of the crack, measurements were carried out. Fig. 7(a) shows the real part of impedance for undamaged and damaged plate (plate 1) for frequency range from 20 to 30 kHz. In order to make effect of intensifying damage on impedance spectrum more visible, this figure is zoomed from frequency 26.5 to 29 kHz (Fig. 7(b)). As it was expected, it can be seen, presence of crack on plate increases local flexibility of the plate at the crack location, and consequently natural frequencies decrease. Therefore, real part of impedance spectra will shift to the left. By increasing the depth of crack, the shift of the natural frequencies to left is increased. Though for some frequencies, natural frequencies decrease by crack generation is not significantly visible (such as at 20.31 and 24.62 kHz), this is because in these frequencies crack is located in nodal point vicinity. In Fig. 8(a), the real part of impedances obtained by theoretical model for undamaged plate and damaged plate with three different crack depths are demonstrated. To make effect of intensifying damage on impedance spectrum evident, this figure is zoomed from frequency 26.5 to 29 kHz (Fig. 8(b)). Similar to the natural frequencies measured by experiments, crack generation will shift the natural frequency to the left and intensifying this crack by increasing its depth will increase this shift. Decreasing natural frequencies by crack depth increasing was expected because in fact generation of crack and increasing crack depth will decrease structural stiffness based on Eq. 33. Similar to experimental results, at some frequencies such as 20.32 and 24.27 kHz, this shift is not significantly obvious. The related numerical data is given in Table 3. By generation of crack and intensifying this crack, same trends can be observed for natural frequencies obtained by theoretical model and experiments.

### 3.3 Effect of damage location and intensity on damage index

In order to examine effect of damage location and

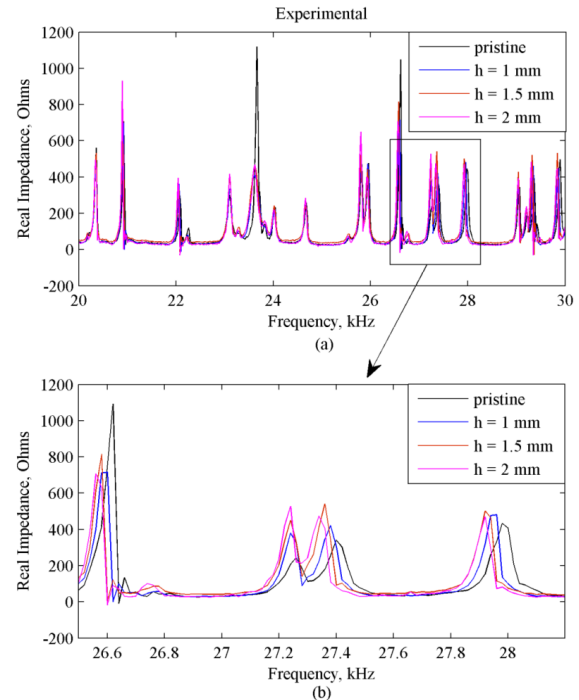


Fig. 7 Impedance real part obtained by experiments for undamaged plate 1 and damaged plate 1 with three different depth of cracks  $h=1$ , 1.5 and 2 mm (a) 20 to 30 kHz (b) 26.5 to 29 kHz

Table 3 Natural frequencies obtained by theoretical model and by experimental tests for damaged plate 1 (from 20 to 30 kHz)

	Experimental Freq. (kHz)	Theoretical Freq. (kHz)	Deviation%
$h=1$ mm	27.79	27.76	0.107
$h=1.5$ mm	27.76	27.73	0.108
$h=2$ mm	27.72	27.70	0.072
$h=1$ mm	27.28	27.22	0.219
$h=1.5$ mm	27.25	27.20	0.183
$h=2$ mm	27.24	27.18	0.220
$h=1$ mm	20.31	20.32	0.049
$h=1.5$ mm	20.31	20.32	0.049
$h=2$ mm	20.30	20.31	0.049

intensity on damage index, three plates 1, 2 and 3 are selected as test specimens. As first step, the tests are carried out on undamaged plates to investigate the similarity of impedance spectrum. As it can be seen in Fig. 9, however the test specimens have been cut from unique plate with same dimensions but the impedance spectrum is not exactly similar and there exists an initial differences between these undamaged plates: the natural frequencies obtained by experimental tests differ almost up to 1.1% for these plates. This is due to not only uncertainties in plate dimensions but also to uncertainties in PWAS dimensions and locations on these plates.

In the second step, in order to examine the effect of damage location, first three initial cracks parallel to  $x$

axis are artificially generated and centered at different positions (Fig. 10 and Table 4). Damages on plate 1 and 3 have farthest and nearest distance to PWAS respectively.

Then to study the effect of damage intensity, the initial generated cracks on these plates are intensified by increasing the depth of crack in three steps:  $h=1, 1.5$  and  $2$  mm. For each location and depth of the crack,

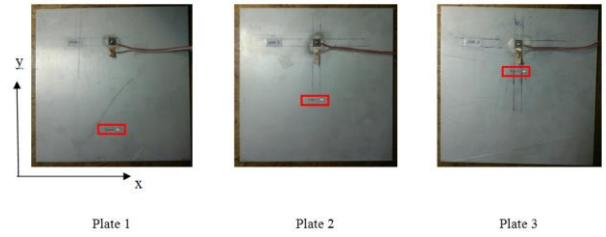


Fig. 10 Photography of damaged plates 1, 2 and 3 with attached PWAS patches

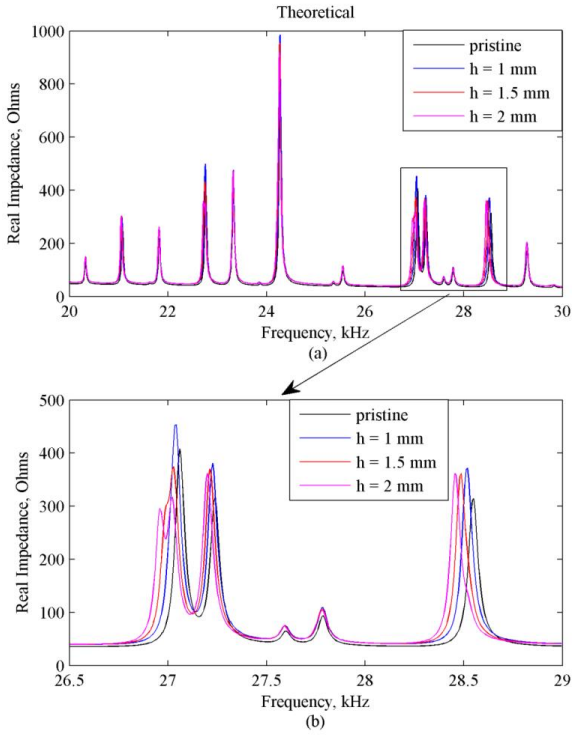


Fig. 8 Impedance real part obtained by theoretical model for undamaged plate and damaged plate with three different depths of cracks  $h=1, 1.5$  and  $2$  mm (a) 20 to 30 kHz (b) 26.5 to 29 kHz

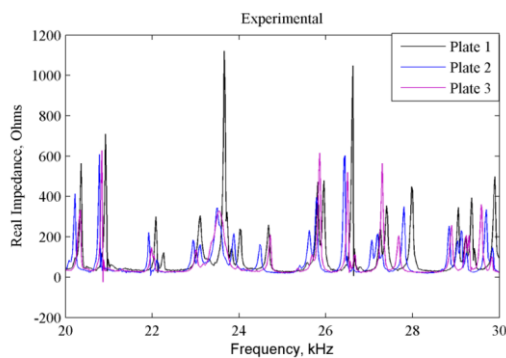


Fig. 9 Real part of PWAS impedance obtained by experiments for undamaged plates 1, 2 and 3

Table 4 Damage locations on Plate 1, 2 and 3

Plate #	Damage position (mm)		Distance to PWAS (mm)
	x	y	
1	100	40	115
2	100	80	75
3	100	120	35

measurements were carried out. While impedance spectrum provides a qualitative approach for damage identification, a scalar quantity can be useful to compare impedance spectra and evaluate severity of damage. For this purpose, three different damage indexes widely used in SHM (Giurgiutiu 2005), are proposed and used in this study. Root mean square deviation (RMSD), the mean absolute percentage deviation (MAPD), and correlation coefficient deviation (CCD) are introduced here to compare damage severity quantitatively which can be determined as follow

$$RMSD = \sqrt{\frac{\sum_{i=1}^N [\text{Re}(Z_{i,1}) - \text{Re}(Z_{i,2})]^2}{\sum_{i=1}^N [\text{Re}(Z_{i,1})]^2}} \quad (34)$$

$$MAPD = \frac{100}{N} \sum_{i=1}^N \left| \frac{\text{Re}(Z_{i,1}) - \text{Re}(Z_{i,2})}{\text{Re}(Z_{i,1})} \right|$$

$$CCD = 1 - \frac{\sum_{i=1}^N [\text{Re}(Z_{i,1}) - \text{Re}(\bar{Z}_{i,1})][\text{Re}(Z_{i,2}) - \text{Re}(\bar{Z}_{i,2})]}{\sigma_{Z,1}\sigma_{Z,2}}$$

Where  $N$  is the number of frequencies in the spectrum, and subscripts 1 and 2 express undamaged and damaged state of the structure respectively.  $\sigma_{Z,1}$  and  $\sigma_{Z,2}$  signify standard deviations. After carrying out the experimental tests on damaged plates, the damage indexes presented by Eq. (33) are calculated. The data processing results in frequency range 20- 30 kHz are listed in Table 5. It can be observed that whatever RMSD, MAPD and CCD is selected, the resulted damage indexes increase with increasing depth of the crack in each plate. For convenient, damage indexes are plotted in Fig. 11. By comparing damage indexes given in Table 5, one can deduced that decreasing damage distance to PWAS affects RMSD and

Table 5 Damage index for three plates and three depth of crack

Depth of crack (mm)	Plate1			Plate2			Plate3		
	1	1.5	2	1	1.5	2	1	1.5	2
RMSD	0.2958	0.3605	0.4084	0.1826	0.2153	0.2766	0.2016	0.2136	0.2288
MAPD	0.0784	0.1287	0.1325	0.0597	0.0723	0.0922	0.0695	0.0709	0.1031
CCD	0.2681	0.392	0.4896	0.1986	0.2291	0.3453	0.1833	0.2019	0.2464

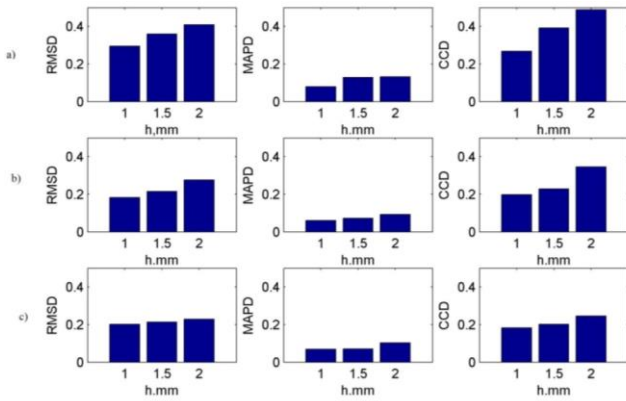


Fig. 11 Damage indexes for (a) plate 1, (b) plate 2, and (c) plate 3

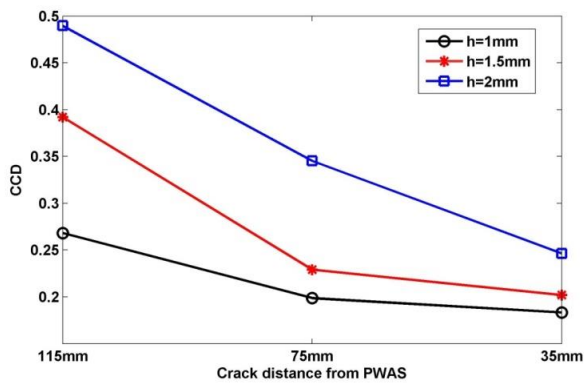


Fig. 12 CCD damage index for severity of crack

MAPD indexes following non justified behavior and almost show a random trend. While by decreasing the crack distance to PWAS (from plate 1 to plate 3), based on experimental results, CCD can be used as an adequate damage index to detect damage severity in SHM (Fig. 12).

#### 4. Conclusions

In this paper, electromechanical impedance model is proposed and developed for undamaged and damaged simply supported rectangular thin aluminum plates. This model is based on flexural vibration of the plate. The theoretical model for electromechanical impedance of PWAS for both undamaged and damaged plate are validated by comparison of theoretical results with experimental ones.

Theoretical and experimental results on cracked plate show that by increasing crack depth, impedance spectra vary by decreasing of structural natural frequency. At some frequencies, natural frequency decrease is not significant; this is because in these frequencies crack is located in nodal point vicinity. RMSD, MAPD and CCD as damage metrics are used to detect damage severity. Comparing these damage indexes based on experimental results demonstrates that increasing crack depth can be detectable by CCD.

The proposed models can be used to investigate the effect of boundary conditions, environmental conditions

such as temperature variation, environmental vibration electromechanical impedance response of plates. The theoretical and experimental results indicate that electromechanical impedance method with adequate damage metric can be a powerful technique with high sensitivity to crack generation and crack intensity in plate structures.

#### References

- Giurgiutiu, V. (2005), "Damage detection in thin plates and aerospace structures with the electro-mechanical impedance method", *Struct. Hlth. Monit.*, **4**(2), 99-118.
- Giurgiutiu, V. and Zagari, A.N. (2002), "Embedded self-sensing piezoelectric active sensors for on-line structural identification", *J. Vib. Acoust.*, **124**(1), 116-125.
- Khadem, S.E. and Rezaee, M. (2000), "Introduction of modified comparison functions for vibration analysis of a rectangular cracked plate", *J. Sound Vib.*, **236**(2), 245-258.
- Lee, J.C., Shin, S.W., Kim, W.J. and Lee, C.J. (2016), "Electromechanical impedance based monitoring for the setting of cement paste using piezoelectricity sensor", *Smart Struct. Syst.*, **17**(1), 123-134.
- Li, G.Q., Chuan-Yao, C. and Yuan-Tai, H. (2005), "Equivalent electric circuits of thin plates with two-dimensional piezoelectric actuators", *J. Sound Vib.*, **286**(1-2), 145-165.
- Liang, C., Sun, F.P. and Rogers, C.A. (1994), "Coupled electro-mechanical analysis of adaptive material systems - determination of the actuator power consumption and system energy transfer", *J. Intel. Mater. Syst. Struct.*, **5**(1), 12-20.
- Lim, Y.Y. and Soh, C.K. (2013), "Damage detection and characterization using EMI technique under varying axial load", *Smart Struct. Syst.*, **11**(4), 349-364.
- Min, J., Yi, J.H. and Yun, C.B. (2015), "Electromechanical impedance-based long-term shm for jacket-type tidal current power plant structure", *Smart Struct. Syst.*, **15**(2), 283-297.
- Min, J., Yun, C.B. and Hong, J.W. (2016), "An electromechanical impedance-based method for tensile force estimation and damage diagnosis of post-tensioning systems", *Smart Struct. Syst.*, **17**(1), 107-122.
- Rugina, C., Enciu, D. and Tudose, M. (2015), "Numerical and experimental study of circular disc electromechanical impedance spectroscopy signature changes due to structural damage and sensor degradation", *Struct. Hlth. Monit.*, **14**(6), 663-681.
- Sepehry, N., Bakhtiari-Nejad, F. and Shamshirsaz, M. (2014), "Thermo-Electro-Mechanical impedance based structural health monitoring of plates", *Compos. Struct.*, **116**, 147-164.
- Sepehry, N., Shamshirsaz, M. and Bastani, A. (2011), "Experimental and theoretical analysis in impedance-based structural health monitoring with varying temperature", *Struct. Hlth. Monit.*, **10**(6), 573-585.
- Tarazaga, P.A., Peairs, D.M., Wilkie, W.K. and Inman, D.J. (2006), "Structural health monitoring of an inflatable boom subjected to simulated micrometeoroid/orbital debris damage", *Proceedings of SPIE 11<sup>th</sup> International Symposium on Nondestructive Evaluation for Health Monitoring and Diagnostics*, San Diego, USA, February.
- Tseng, K.K. and Wang, L. (2005), "Structural damage identification for thin plates using smart piezoelectric transducers", *Comput. Method. Appl. Mech. Eng.*, **194**(27-29), 3192-3209.
- Wang, X., Ehlers, C. and Neitzel, M. (1996), "Electro-mechanical dynamic analysis of the piezoelectric stack", *Smart Mater. Struct.*, **5**(4), 492-500.

- Wang, X., Ehlers, C. and Neitzel, M. (1997), "An analytical investigation of static models of piezoelectric patches attached to beams and plates", *Smart Mater. Struct.*, **6**(2), 204-213.
- Yan, W., Chen, W.Q., Cai, J.B. and Lim, C.W. (2007), "Quantitative structural damage detection using high-frequency piezoelectric signatures via the reverberation matrix method", *Int. J. Numer. Method. Eng.*, **71**(5), 505-528.
- Zagrai, A.N. and Giurgiutiu, V. (2001), "Electro-mechanical impedance method for crack detection in thin plates", *J. Intel. Mater. Syst. Struct.*, **12**(10), 709-718.

HJ

## Appendix A

$$Q_1 = \frac{1}{\rho H} \left[ \frac{e_1 b}{\beta_m} I_{hy} \frac{dF_1}{dx} \Big|_{x_1}^{x_2} - \frac{e_2 b}{\gamma_m} I_y \frac{dF_2}{dx} \Big|_{x_1}^{x_2} \right],$$

$$Q_2 = \frac{1}{\rho H} \left[ \frac{e_1 \beta_m}{b} I_{hy} \int_{x_1}^{x_2} F_1 dx + \frac{e_1 \beta_m}{b} I_y \int_{x_1}^{x_2} F_2 dx \right],$$

where

$$F_1 = 1, \quad F_2 = \frac{e_3 + e_4 E(x/a) f(x/a)}{e_5 E(x/a) f(x/a)}$$

$$I_y = \cos \gamma_m \frac{y_2 - b}{b} - \cos \gamma_m \frac{y_1 - b}{b},$$

$$I_{hy} = \cosh \beta_m \frac{y_2 - b}{b} - \cosh \beta_m \frac{y_1 - b}{b}$$

$$A_2 = \frac{-H/2}{\omega_{cnn}^2 - \omega^2 + 2\omega_{cnn}\omega\zeta_f j} \left\{ \frac{e_1 \beta_m}{a_p b} I_{hy} \int_{x_1}^{x_2} F_1 dx + \frac{e_2 \gamma_m}{a_p b} I_y \int_{x_1}^{x_2} F_2 dx \right\}.$$

$$A_1 = \frac{-H/2}{\omega_{cnn}^2 - \omega^2 + 2\omega_{cnn}\omega\zeta_f j} \left\{ \frac{be_1}{b_p \beta_m} I_{hy} - \frac{e_2 b}{b_p \gamma_m} I_y \frac{dF_2}{dx} \Big|_{x_1}^{x_2} \right\}.$$